

Adiabatic Heavy Ion Fusion Potentials for Fusion at Deep Sub-barrier Energies

S. V. S. Sastry, S.Kailas, A. K. Mohanty and A. Saxena

Nuclear Physics Division, Bhabha Atomic Research Centre, Trombay, Mumbai 400 085, India

(Dated: December 10, 2018)

It is shown that the energy (E) and angular momentum (L) dependent barrier penetration model (ELDBPM) provides a consistent description of the unusual behaviour of fusion cross sections at extreme sub-barrier energies reported recently. The adiabatic limit of fusion barriers derived from experimental data are consistent with the adiabatic fusion barriers given by modified Wilzyska-Wilzynski prescription. Using the ELDBPM , the fusion barrier systematics has been obtained for a wide range of heavy ion systems. For some systems, the barrier parameters R_b and $\hbar\omega$ are anomalously smaller than the predictions of known empirical prescriptions.

PACS numbers: PACS Nos. 25.70Jj, 24.10.Eq

Keywords: Heavy ions fusion, Fusion barrier systematics, Energy dependent barrier, Adiabatic and Sudden barriers, Fusion Slope function.

Heavy ions fusion has been under intense investigation over the last two decades. Heavy ions fusion populates compound system at high excitation energies and angular momenta, providing a tool to study the nucleus at extreme conditions. It also opens up a new channel to generate nuclei far away from stability line, populate the super heavy nuclei near the island of stability. Further, the fusion of heavy ions at sub Coulomb barrier energies exhibited anomalously large enhancements over the model estimates based on tunneling of the entrance channel Coulomb barrier. This enhancement has been understood to be arising due to the strong coupling of structure of the fusing nuclei and the reaction dynamics [1]. The effects couplings of nuclear structure on fusion has been clearly brought out in the experimental studies of the fusion barrier distributions [2] and see the references in [2]. These dynamical aspects of heavy ion reactions are successfully explained by the coupled reaction channels (CRC) formalism, by a simultaneous solution to all the reaction channels as in [3]. Nuclear fusion at extreme sub-barrier energies has been revisited recently [4, 5]. Jiang *et. al.* [4] have reported unexpected behaviour of fusion cross sections at extreme sub-barrier energies. The Wong model results fail to reproduce the data at these low energies. They have observed that the logarithmic slope ($L(E) = \frac{d \ln(E\sigma)}{dE}$) increases with decrease of energy in contrast to a constant value expected at the deep sub-barrier energies. Hagino *et. al.*, [5] have pointed out that the failure of the Wong model analysis to explain the unexpected behaviour of fusion cross sections shown by Jiang *et. al.*, [4] is partly due to the parabolic shape of the fusion barrier assumed in the Wong model. Further, Hagino *et. al.*, [5] noted that the increase in logarithmic slope with decreasing energy is consistent with the large diffuseness parameter required to fit the recent high precision fusion data. In the present work, we have investigated the unusual behaviour of fusion at deep sub-barrier energies and also the systematics of adiabatic limit of fusion barriers in terms of the energy (E) and angular momentum (L) dependent barrier penetration model (ELDBPM) [6].

Owing to complexity of the CRC calculations, phenomenological models are needed to gain physical insight of the reaction mechanism. The effective potentials derived from the CRC method provide an important bridge between the microscopic CRC calculations and the macroscopic models. It has been shown that the CRC fusion cross sections and the spin distributions imply an effective fusion barrier that depends on both E and L through effective radial kinetic energy defined (see Eq. 2.) as $\epsilon = E - E_{rot}$ [6]. Analysis of experimental data using ϵ dependent barrier showed two distinct limits for the effective fusion potentials. At high energies (above E_2) well above uncoupled elastic channel barrier, fusion occurs by transmission through a single constant barrier known as sudden fusion barrier (V_2). As the energy decreases and/or the angular momentum increases, the effective fusion barrier decreases linearly with ϵ until a lower energy (E_1) is reached. At this lower limit called adiabatic limit, fusion occurs by tunneling through a constant barrier known as adiabatic fusion barrier (V_1) [6, 7]. This simple effective fusion barrier model was first proposed in [7], based on the neck degree of freedom in heavy ion fusion. The two dimensional potential energy landscape as a function of relative separation and neck degree exhibits two distinct regions [7]. At high energies, the colliding nuclei in the entrance channel fuse by passage over the relative Coulomb barrier in the radial space. As the energy is lowered the fusing system finds an alternate competing path for fusion by means of neck formation. Thus the neck formation facilitates the fusion in a dynamic way, which otherwise has to fuse by passage through the one dimensional barrier. At very low energies, the effects of neck opening saturate and system fuses by transmission through a lowered (constant) barrier. The effective fusion barrier (V_{eff}), the transmission factor for fusion (T_l), the fusion cross section

(σ_f), the mean square fusion spin ($\langle L^2 \rangle$) values and the fusion slope values ($L(E)$) using the ELDBPM [6] are,

$$\begin{aligned} V_{eff}(\epsilon) &= V_2 \quad \text{for } \epsilon \geq E_2 \\ V_{eff}(\epsilon) &= \alpha\epsilon + \beta \quad \text{for } E_1 \leq \epsilon \leq E_2 \\ V_{eff}(\epsilon) &= V_1 \quad \text{for } \epsilon \leq E_1 \end{aligned} \quad (1)$$

$$\epsilon = E - E_{rot} \quad \text{where} \quad E_{rot} = \frac{l(l+1)\hbar^2}{2\mu R_b^2} \quad (2)$$

$$\sigma_l = \frac{\pi}{k^2}(2l+1)T_l(E) \quad (3)$$

$$T_l(E) = \left[1 + \exp\left(\frac{2\pi}{\hbar\omega}(V_{eff} - \epsilon)\right) \right]^{-1} \quad (4)$$

$$\sigma_f = \sum_l \sigma_l \quad \text{and} \quad \langle L^2 \rangle = \sum_l l(l+1)\sigma_l/\sigma_f \quad (5)$$

$$L(E) = \frac{d \log(\sigma E)}{dE} \quad (6)$$

In Eq. (1), $\alpha = (V_2 - V_1)/(E_2 - E_1)$ and $\beta = -\alpha E_1 + V_1$. This simple model for fusion consists of all the physical ingredients of the CRC calculations [6]. Further, the results of EDBPM with L-independent barriers [7] can be obtained by substituting E_{cm} in place of ϵ dependence of V_{eff} . In the following, both ELDBPM and EDBPM will be used to understand the heavy ion fusion systematics. In the above equations, the quantities R_b , and $\hbar\omega$ are in general taken independent of energy. However, these quantities may be different at the sudden and adiabatic limits. The sudden limit of the barrier is generally around the one dimensional fusion barrier, as prescribed by Vaz *et. al.*, [8] (see Eq. 7). The contact radius (R_{con}) is the distance between two touching spheres evaluated by using $r_0=1.233\text{fm}$.

$$\begin{aligned} R_{sud} &= r_{of}(A_p^{1/3} + A_t^{1/3}) \\ r_{ef} &= 2.2951 - 0.2966 \log_{10}(Z_p Z_t) \\ r_{of} &= 2.0513 - 0.2455 \log_{10}(Z_p Z_t) \\ V_{sud} &= \frac{Z_p Z_t e^2}{r_{ef}(A_p^{1/3} + A_t^{1/3})} \end{aligned} \quad (7)$$

Wilzynsky and Wilzynska showed that the adiabatic limit of the fusion barrier can be obtained in terms of the ground state masses of the fusing nuclei and the fused system [9]. In this prescription, the depth of the nucleus-nucleus (NN) potential in the adiabatic limit is given by the potential of the compound nucleus calculated with respect to the potential energy of the two separated incident nuclei of entrance channel with their Coulomb energy (C_0 in MeV) subtracted. Thus, the depth V_0 (in MeV) of a Woods-Saxon form of the NN potential in the adiabatic limit is given by, $V_0 = (M_p + M_t - M_{cn})c^2 + C_0$. Recently, Wilzynska and Wilzynsky modified the above prescription by considering shell correction term for the compound nucleus [10]. The shell correction energy (S_{cn}) is taken from the Moller and Nix *et. al.*, [11]. In general, this term is found to lower the adiabatic barriers. As mentioned in [10], this shell correction term is necessary because it produces only a local dip in the flat landscape of the nuclear potential energy for the equilibrium shapes. The diffuseness parameter (a_0) of the potential can be determined by matching the first derivative of the NN potential (i.e., NN force) to that of the proximity potential at the contact distance $R_0=R_p + R_t$. A correlation between the adiabatic barriers and the fusion energy thresholds was shown in [10] over a wide range of heavy ion systems. This fusion threshold energy is defined as the energy at which measured fusion cross section is equal to the s-wave absorption cross section.

$$V_0 = (M_p + M_t - M_{cn})c^2 + C_0 + S_{cn} \quad (8)$$

$$C_0 = 0.7054 \left(\frac{Z_{cn}^2}{A_{cn}^{1/3}} - \frac{Z_p^2}{A_p^{1/3}} - \frac{Z_t^2}{A_t^{1/3}} \right) \quad (9)$$

$$V_{NN}(r) = \frac{-V_0}{1 + \exp\left(\frac{r-R_0}{a_0}\right)} \quad (10)$$

$$\left. \frac{dV_{NN}}{dr} \right|_{r=R_0} = \frac{-V_0}{a_0} = 16\pi\gamma \frac{R_p R_t}{R_p + R_t} \quad (11)$$

In the above equations, γ is the surface tension coefficient, r_0 is the radius parameter. In [9, 10], these are taken to be $\gamma = 0.9516 \left[1 - 1.7826 \left(\frac{N-Z}{A} \right)^2 \right] \text{MeV}/\text{fm}^2$, $r_0=1.15\text{fm}$. The adiabatic barriers obtained from the prescription of

[10] using these γ and r_0 are shown in the Table 1 in second column (V_{ad}) for various systems listed in column 1. The corresponding barrier radius (R_b), barrier curvature ($\hbar\omega$) and the potential diffuseness at adiabatic limit are given in Table in columns 3 to 5. The diffuseness parameter of NN potential turns out to be around 0.90-1.20 fm as shown in the Table. Such larger diffuseness values, reported in some of the fusion studies [2], arise naturally in the prescription of adiabatic barriers. In order to verify this empirical prescription of [10], it is necessary to determine the adiabatic fusion barriers using experimental data. Further, the shell correction prescription needs to be examined in detail by studying the isotopic dependence of adiabatic barriers. Therefore, we have derived the adiabatic barriers using the ELDBPM fits to the experimental fusion data of some heavy ion systems with $Z_p Z_t$ values ranging from 400 to 1100.

The best fit parameters of ELDBPM, $E_2, V_2, E_1, V_1, R_b, \hbar\omega$ and the χ^2 values of fits are listed in columns 10 to 16 of Table. The resulting fits to fusion excitation functions are shown in Figure 1, with solid curves and the experimental data by symbols for the 26 systems considered in this work. The experimental data for these systems are taken from [4, 12, 13, 14, 15, 16, 17, 18, 19]. The V_1 values listed in the Table in column 13 are the adiabatic barriers derived from the experimental data for all these cases. These V_1 values do not agree with the adiabatic barriers given in column 2 of Table and therefore, the prescription of [10] under predicts the V_1 values. It is observed that the values of r_0 and γ of [10] are different from the values used in compilations of Moller *et. al.*, [11], where $\gamma = 1.25 \left[1 - 2.3 \left(\frac{N-Z}{A} \right)^2 \right] \text{ MeV/fm}^2$ based on $r_0 = 1.16 \text{ fm}$. Therefore, we have taken these values of r_0 and γ consistent with nuclear data compilations. The ground state masses and shell correction energy are also taken from [11]. The resulting empirical adiabatic barrier parameters V_{ad} , R_b , $\hbar\omega$ and the diffuseness are listed in the columns 6-9 of the Table. 1. These V_{ad} values are very close to the V_1 values of column 13. The isotopic variation for a given $Z_p Z_t$ are grouped together and are separated by a horizontal line in the Table. The isotopic dependence of the adiabatic barriers is very well reproduced in the present work. The diffuseness parameters are in the range of 0.65-0.9fm as shown in 9th column of Table, in contrast to the diffuseness values of [10] (see column 5). The effective diffuseness of the NN potential in the adiabatic limit is reduced by our choice of the surface tension parameter, leading to correct adiabatic barriers [20]. Consequently, the $\hbar\omega$ values in the adiabatic limit are slightly larger than those of [10] (columns 8 and 4 of Table.)

Figure 2(a) shows the ELDBPM fits to fusion cross sections for the $^{58}\text{Ni}+^{58}\text{Ni}$ system in solid curves. The experimental data of [4, 12] is shown by circles, showing the good quality of the model fits. In Figure 2(b) we show the ELDBPM fits to the fusion excitation function of $^{60}\text{Ni}+^{89}\text{Y}$. The fusion of this system has been shown to exhibit anomalously steeper fall in deep sub barrier region as compared to Wong's model estimates and coupled channels method. It can be seen that in the ELDBPM, the cross section at deep sub-barrier region is reproduced. The best fit values are respectively $R_b=8.75\text{fm}$ and $\hbar\omega=2.75\text{MeV}$ for $^{58}\text{Ni}+^{58}\text{Ni}$ system and $R_b=8.0\text{fm}$ and $\hbar\omega=2.50\text{MeV}$ for $^{60}\text{Ni}+^{89}\text{Y}$. These values are lower than the values predicted by the prescription of [10] for these two systems (see Table).

We have calculated the exponential slope parameter given by Eq. 6. The slope values $L(E)$ for these two systems are shown in Figs.2(c,d). The experimental slope values are well reproduced in the present work as shown in figure, except at the lowest energies. These maximum slope values could not be reproduced, in spite of using very low value $\hbar\omega$ ($=2.5\text{MeV}$). Exact WKB transmission in place of transmission through parabolic barrier would tend to increase the theoretical model values of slope at low energy, as shown in [5].

The percentage deviations of adiabatic barrier heights (V_1) derived in the present work as compared to the modified prescription of [10] have been calculated for the systems shown in Table. The percentage deviations of sudden barrier heights (V_2) are compared to the phenomenological formulae given by Vaz *et. al.*, [8]. These are shown in (left side of) Figures 3(a,b) as a function of $Z_p Z_t$, which is a measure of heavyness of the system. As shown in Figure 3(a), the deviations of V_1 for all these systems are within 2%, where as the deviations of V_2 are upto 6%. The solid line drawn in the figures shows general trend of $Z_p Z_t$ dependence of these deviations, obtained by a 2^{nd} order polynomial fit.

The optimised R_b values that fit the fusion data of Fig. 1 are listed in column 14 of the Table. These values have been plotted in Figure 3(c) (left part) as a function of $Z_p Z_t$. For a comparison, the adiabatic barrier radii, the sudden values as given by Vaz *et. al.*, [8] and the contact radii (R_{con}) are shown by different symbols. For some systems, the required R_b values are much smaller than the sudden, adiabatic and contact radii values. The solid and dashed curves are polynomial fits to data showing general trends. It should be noted that the ELDBPM parameters listed in Table are a result of a uniform procedure applied to all systems. Further, the R_b and $\hbar\omega$ values are independent of energy and angular momentum and therefore they are effective parameters. These parameters also should be varied between their sudden and adiabatic limit values in an ϵ dependent way, similar to effective barrier of Eq. (1). Such an implicit E and L dependence of $\hbar\omega$ mimics the true WKB transmission.

Similar analysis was performed using EDBPM method where the effective fusion barrier depends only on E_{cm} and hence without L-dependence. The results of fusion barrier systematics in EDBPM analysis are shown in right panel of Fig.3. The fits to fusion excitation functions and resulting fusion slope values of EDBPM are very similar to the

those in Figs. (1,2).

As shown in Fig.3(c), the values of R_b derived in the present work are smaller than the values expected from high energy systematics given by Vaz *et. al.*. In order to understand this behaviour, we have analysed the high energy fusion data of a few systems by a one dimensional BPM. We performed a three parameter fit to above barrier fusion data by optimising V_b, R_b and $\hbar\omega$. For some systems like $^{36}\text{S}+^{58}\text{Ni}$, the R_b values turn out to be smaller. For the $^{58}\text{Ni}+^{58}\text{Ni}$ this procedure yields a slightly higher value than the ELDBPM values (listed in table). In the high energy region above E_2 , fusion can be obtained by $\sigma_f = \pi R_b^2(1 - V_b/E)$. Therefore, the smallness of R_b is a requirement of the high energy fusion cross sections for some of the systems.

The $\hbar\omega$ values are important for deep sub barrier data and are closer to the empirical adiabatic values listed in Table. The smallness of $\hbar\omega$ is system dependent, especially as shown for the cases of $^{36}\text{S}+^{58}\text{Ni}$ and $^{58}\text{Ni}+^{58}\text{Ni}$, where fusion data extends to deep sub barrier region. The optimised $\hbar\omega$ values the Ar+Sm systems are around 5MeV (see Table). Though these systems have $Z_p Z_t$ values similar to Ni+Y system, the barrier curvatures are very different. These observations may be understood based on neck degree of freedom for fusion. In the macroscopic picture, fusion occurs by both the barrier penetration in radial space and neck opening. The barrier curvature depends on the reduced mass. The mass tensor is a complex quantity and depends on size of the system as well as structural details of the colliding nuclei. The neck formation is more favourable for heavier systems and the mass tensor is smaller, resulting in larger $\hbar\omega$ values. Often, neutron flow is also considered to be a classical analogue of neck opening. Consequently, the $\hbar\omega$ can be larger even for a light system, whenever neutron flow is favoured.

In order to confirm the anomalous small values of R_b and $\hbar\omega$, study of systematics of fusion at high energy is very important. Therefore, we used the program CCFUS [21] to fit the high energy fusion data without any couplings. The parameter dV of CCFUS is adjusted to fit the cross sections above 100mb for each system (except for Kr+Ge systems which could not be reproduced). The resulting barrier height, R_b and $\hbar\omega$ and the dV values used are listed in the Table in the last four columns. It can be seen that this high energy systematics from CCFUS also yields smaller R_b and $\hbar\omega$ values. However, the barrier heights obtained by this procedure represent the uncoupled entrance channel barriers. In the coupled channels method [1], these high energy barriers are also modified by the couplings.

Acknowledgements

We acknowledge fruitful discussions with B. K. Nayak, R. G. Thomas, P. K. Sahu and K. Mahata.

Conclusion

The fusion cross sections from well above barrier to extreme sub-barrier energies have been analysed using the energy (E) and angular momentum (L) dependent barrier penetration model (ELDBPM). From this analysis, the adiabatic limits of fusion barriers have been determined for a wide range of heavy ion systems. The empirical prescription of Wilzynska and Wilzynski has been used with modified radius parameter and surface tension coefficient values consistent with the parameterization of the nuclear masses. The adiabatic fusion barriers calculated from this prescription are in good agreement with the adiabatic barriers deduced from ELDBPM fits to fusion data. The nuclear potential diffuseness is larger at adiabatic limit, resulting in a lower $\hbar\omega$ leading to increase of "logarithmic slope" observed at energies well below the barrier. The effective fusion barrier radius and curvature values are anomalously smaller than the predictions of known empirical prescriptions. A detailed comparison of the systematics of fusion barrier with and without L-dependence has been presented.

-
- [1] C. H. Dasso, S. Landowne and A. Winther, Nucl. Phys. **A405**, 381 (1983).
 - [2] M. DasGupta, D. J. Hinde, N. Rowley and A. M. Stefanini, Annu. Rev. Nucl. Part. Sci **48**, 401 (1998)
 - [3] I. J. Thompson, Computer Phys. Rep. **7**, 167 (1988)
 - [4] C. L. Jiang, H. Esbensen, K. Rehm *et. al.*, , Phys. Rev. Lett. **89** 052701 (2002).
 - [5] K. Hagino, N. Rowley and M. Dasgupta, Phys. Rev. **C67**, 054603, (2003).
 - [6] A. K. Mohanty, S.V.S. Sastry, S. K. Kataria and V.S. Ramamurthy, Phys. Rev. Lett. **65**, 1096, (1990); *ibid.* Phys. Rev. **C46**, 2012, (1992).
 - [7] V.S. Ramamurthy, A. K. Mohanty, S. K. Kataria and G. Rangarajan, Phys. Rev. **C41**, 2702, (1990).
 - [8] L. C. Vaz, J. M. Alexander and G. R. Satchler, Phys. Rep. **69**, 373 (1981).
 - [9] J. Wilzynski and K. Siwek-Wilzynska, Phys. Lett **55B**, 270 (1975); K. Siwek-Wilzynska and J. Wilzynski, Phys. Lett **74B**, 313 (1978).; J. Wilzynski, Nucl. Phys. **A216**, 386 (1973).
 - [10] K. Siwek-Wilzynska and J. Wilzynski, Phy. Rev. **C64**, 024611 (2001);
 - [11] P. Moller, J. R. Nix, W. D. Myers and W. J. Swiatecki, At. Data and Nucl. Data Tables **59**, 185 (1995).

System	$V_{ad}[10]$	R_b	$\hbar\omega$	a_0	V_{ad}	R_b	$\hbar\omega$	a_0	E_2	V_2	E_1	V_1	R_b	$\hbar\omega$	χ^2	V_{cef}	R_b	$\hbar\omega$	dV
$^{28}\text{Si}+^{58}\text{Ni}$	50.0	10.3	3.2	0.86	52.9	9.9	3.9	0.65	56.6	55.6	51.6	52.4	9.0	3.2	1.7	55.0	9.4	3.6	-5.0
$^{28}\text{Si}+^{62}\text{Ni}$	48.6	10.6	2.5	0.90	51.6	10.2	3.7	0.68	59.0	56.8	49.5	50.5	9.2	2.5	1.9	54.1	9.7	3.7	0.0
$^{28}\text{Si}+^{64}\text{Ni}$	47.6	10.8	2.8	0.94	50.7	10.3	3.5	0.71	56.3	55.2	49.4	50.0	8.8	2.8	1.7	54.3	9.6	3.6	-5.0
$^{32}\text{S}+^{58}\text{Ni}$	56.1	10.4	3.2	0.89	59.3	10.1	3.8	0.67	62.1	61.5	58.7	59.0	8.8	3.2	5.5	64.8	9.0	2.6	-16.0
$^{32}\text{S}+^{64}\text{Ni}$	53.1	11.0	3.5	0.99	56.5	10.6	3.4	0.75	64.5	62.5	55.7	56.5	8.8	3.5	11.3	63.8	9.1	2.5	-18.0
$^{36}\text{S}+^{58}\text{Ni}$	54.1	10.8	4.0	0.94	57.4	10.4	3.5	0.71	64.6	63.8	58.8	58.0	8.0	4.0	5.6	64.0	9.0	2.1	-19.0
$^{36}\text{S}+^{64}\text{Ni}$	52.5	11.1	2.5	0.98	55.8	10.7	3.2	0.74	63.4	59.4	54.8	56.0	8.8	2.5	4.1	61.8	9.6	3.0	-15.0
$^{36}\text{S}+^{90}\text{Zr}$	73.2	11.4	3.2	0.98	77.2	11.1	3.5	0.75	80.4	78.8	75.8	76.6	11.2	3.2	93.0	77.6	11.2	3.9	45.0
$^{36}\text{S}+^{96}\text{Zr}$	70.7	11.8	3.0	1.05	74.8	11.4	3.2	0.80	82.0	79.8	73.3	74.1	11.8	3.0	110.8	75.6	11.5	3.8	70.0
$^{40}\text{Ar}+^{112}\text{Sn}$	98.2	11.9	5.0	1.06	103.2	11.6	3.5	0.81	107.4	106.4	100.7	102.5	9.5	5.0	16.9	109.9	11.0	3.7	0.0
$^{40}\text{Ar}+^{116}\text{Sn}$	97.0	12.0	5.0	1.09	102.0	11.8	3.4	0.83	115.1	113.7	100.5	102.3	11.8	5.0	117.4	109.2	11.1	3.6	0.0
$^{40}\text{Ar}+^{122}\text{Sn}$	95.4	12.2	5.0	1.12	100.3	11.9	3.3	0.85	112.7	109.9	99.2	101.4	10.8	5.0	19.2	107.3	11.3	3.7	5.0
$^{40}\text{Ar}+^{144}\text{Sm}$	118.3	12.2	4.0	1.08	123.6	12.0	3.5	0.83	133.1	130.1	120.1	122.3	9.5	4.0	50.5	130.3	11.5	3.8	5.0
$^{40}\text{Ar}+^{148}\text{Sm}$	116.1	12.4	5.0	1.13	121.6	12.2	3.4	0.86	131.0	129.0	116.7	120.5	9.5	5.0	35.8	129.6	11.6	3.8	5.0
$^{40}\text{Ar}+^{154}\text{Sm}$	113.6	12.7	5.0	1.19	119.2	12.4	3.2	0.91	128.4	127.8	112.9	116.3	10.0	5.0	85.2	129.4	11.6	3.6	0.0
$^{46}\text{Ti}+^{90}\text{Zr}$	97.3	11.7	3.8	1.08	102.4	11.4	3.4	0.81	113.3	110.7	99.7	102.1	10.5	3.8	3.3	111.6	10.4	3.1	-10.0
$^{46}\text{Ti}+^{93}\text{Nb}$	98.6	11.8	5.0	1.10	103.9	11.5	3.3	0.84	110.9	109.7	100.2	103.6	10.2	5.0	5.6	113.8	10.5	3.1	-10.0
$^{50}\text{Ti}+^{90}\text{Zr}$	96.8	11.8	4.0	1.06	101.7	11.5	3.3	0.80	108.8	106.8	101.6	103.0	10.2	4.0	1.9	110.1	10.6	3.1	-10.0
$^{50}\text{Ti}+^{93}\text{Nb}$	98.4	11.9	4.0	1.07	103.4	11.6	3.3	0.82	111.0	109.4	101.9	103.9	10.2	4.0	2.5	112.3	10.7	3.1	-10.0
$^{58}\text{Ni}+^{58}\text{Ni}$	91.9	11.1	2.8	0.97	96.5	10.8	3.7	0.74	104.5	103.1	94.2	95.4	8.8	2.8	13.4	103.2	10.0	3.1	-10.0
$^{58}\text{Ni}+^{64}\text{Ni}$	87.6	11.6	4.2	1.07	92.5	11.3	3.3	0.81	99.5	98.7	91.2	93.0	8.2	4.2	13.2	101.2	10.3	3.2	-10.0
$^{64}\text{Ni}+^{64}\text{Ni}$	86.0	11.8	3.0	1.08	90.8	11.5	3.1	0.82	98.5	97.5	90.5	91.5	9.0	3.0	2.9	99.4	10.5	3.1	-10.0
$^{60}\text{Ni}+^{89}\text{Y}$	118.3	11.9	2.5	1.10	124.0	11.7	3.3	0.83	135.2	133.0	123.5	125.5	8.0	2.5	43.7	135.3	10.6	2.3	-13.0
$^{64}\text{Ni}+^{100}\text{Mo}$	121.7	12.4	4.3	1.18	127.9	12.2	3.1	0.90	142.7	142.1	128.6	130.6	11.0	4.3	2.9	140.6	11.1	2.8	-10.0
$^{86}\text{Kr}+^{70}\text{Ge}$	119.9	12.3	3.5	1.19	126.1	12.1	3.0	0.91	141.8	139.0	123.8	126.2	8.0	3.5	81.6	140.9	10.6	1.4	-15.0
$^{86}\text{Kr}+^{76}\text{Ge}$	119.6	12.4	4.5	1.16	125.4	12.2	3.0	0.89	132.9	131.9	124.3	126.5	8.0	4.5	133.8	138.9	10.8	1.8	-15.0

TABLE I: The fusion barrier parameters in the adiabatic limit for various heavy ion systems obtained from the prescription of [10]. The barrier quantities in the 2^{nd} - 5^{th} columns are for parameters $r_0=1.15\text{fm}$, $\gamma=0.9516(1-1.7826I^2)$. The results obtained by using $r_0=1.16\text{fm}$, $\gamma=1.25(1-2.3I^2)$ are given in the 6^{th} - 9^{th} columns, with $I=\frac{N-Z}{A}$. The experimentally derived barrier parameters using ELDBPM analysis, $E_2, V_2, E_1, V_1, R_b, \hbar\omega$ and the χ^2 values are listed in columns 10 to 16. The parameters $V_b, R_b, \hbar\omega$ and dV obtained by fitting high energy fusion data i.e., above 100mb using CCFUS program are given in last four columns. In the table, R_b and a_0 are in units of fm and the others are in MeV.

- [12] M. Backerman, M. Salomaa, A. Sperduto, *et. al.*, Phys. Rev. Lett. **45**, 1472, (1980) ; M. Backerman, J. Ball, H. Enge, *et. al.*, Phys. Rev. **C23**, 1581, (1981).
- [13] M. Backerman, M. Salomaa, A. Sperduto, *et. al.*, Phys. Rev. **C25**, 837, (1982).
- [14] A. M. Stefanini, G. Fortuna, R. Pengo, *et. al.*, Nucl. Phys. **A456**, 509 (1986).
- [15] A. M. Stefanini, L. Corradi, A. M. Vinod Kumar, *et. al.*, Phys. Rev. **C62**, 014601 (2000).
- [16] W. Reisdorf, F. P. Hessberger, K. D. Hilderbrand, *et. al.*, Nucl. Phys. **A438**, 212 (1985).
- [17] P. H. Stelson, H. J. Kim, M. Backerman, *et. al.*, Phys. Rev. **C41**, 1584 (1980).
- [18] J. Halbert, J. R. Beene, D. C. Hensley, *et. al.*, Phys. Rev. **C40**, 2558 (1989).
- [19] W. Reisdorf, F. P. Heissberger, K. D. Hilderbrand *et. al.*, Nucl. Phys. **A444**, 154 (1985).
- [20] S. V. S. Sastry, Ph. D., Thesis submitted to University of Mumbai, 1996 pages 50-52.
- [21] C. H. Dasso, S. Landowne, Comput. Phys. Commun. **46**, 187 (1987).

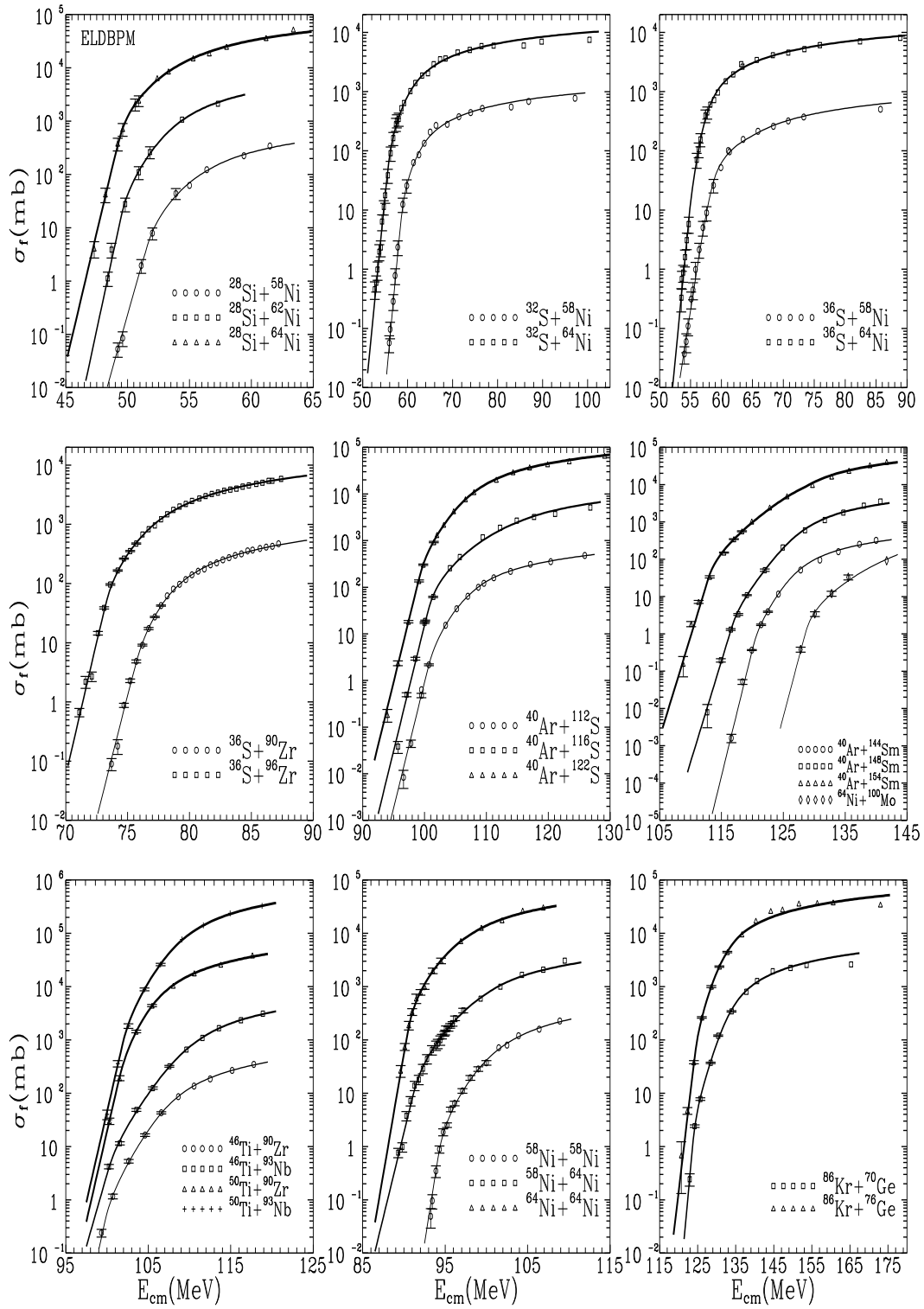


FIG. 1: Fusion excitation functions for the systems shown in Table. 1. For clarity, the fusion data of systems within a graph inset are successively scaled up by a decade. The experimental fusion data are shown by symbols and the solid curves are ELDBPM fits.

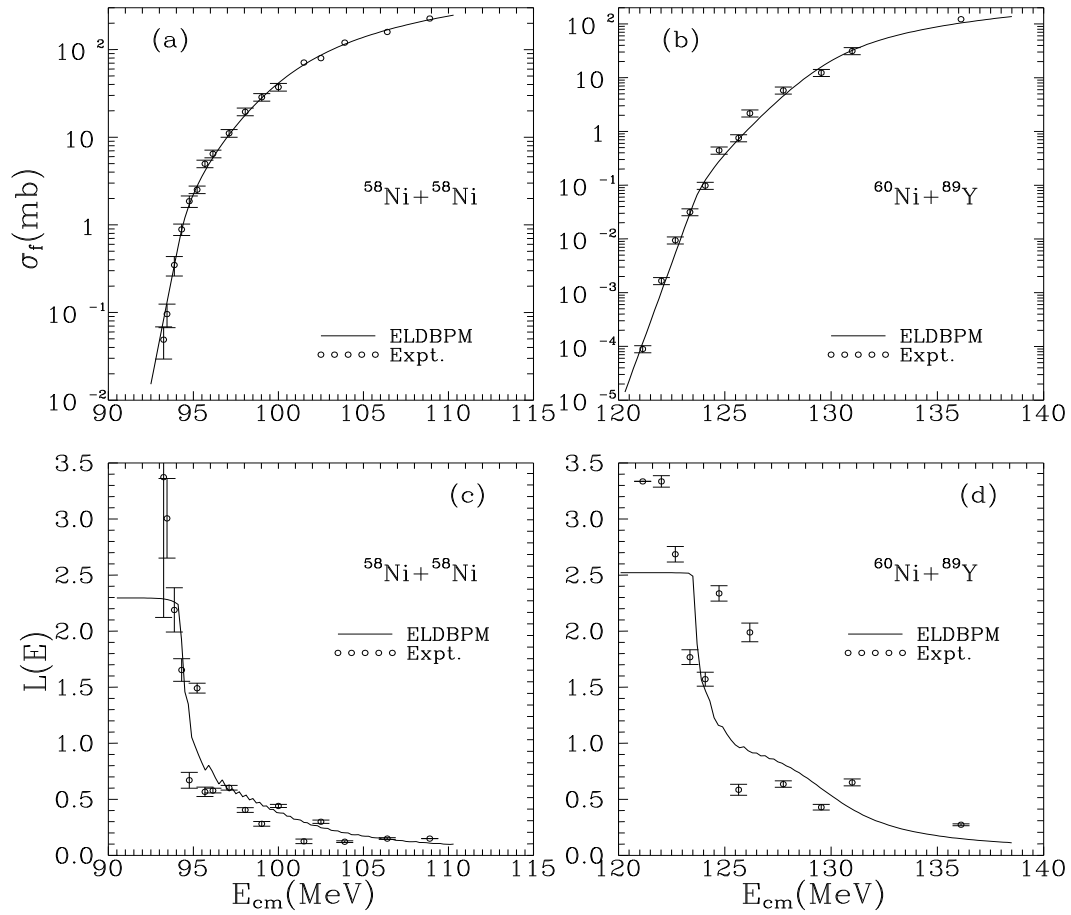


FIG. 2: Fusion excitation function for (a) $^{58}\text{Ni} + ^{58}\text{Ni}$ and (b) $^{60}\text{Ni} + ^{89}\text{Y}$ systems. The experimental fusion data are shown by circles and the solid curves are ELDBPM fits. Fusion slope function defined in [4] for these two systems are shown in Figs. (c,d) respectively. The experimental fusion slope data are shown by circles with error bars and the solid curves are ELDBPM results.

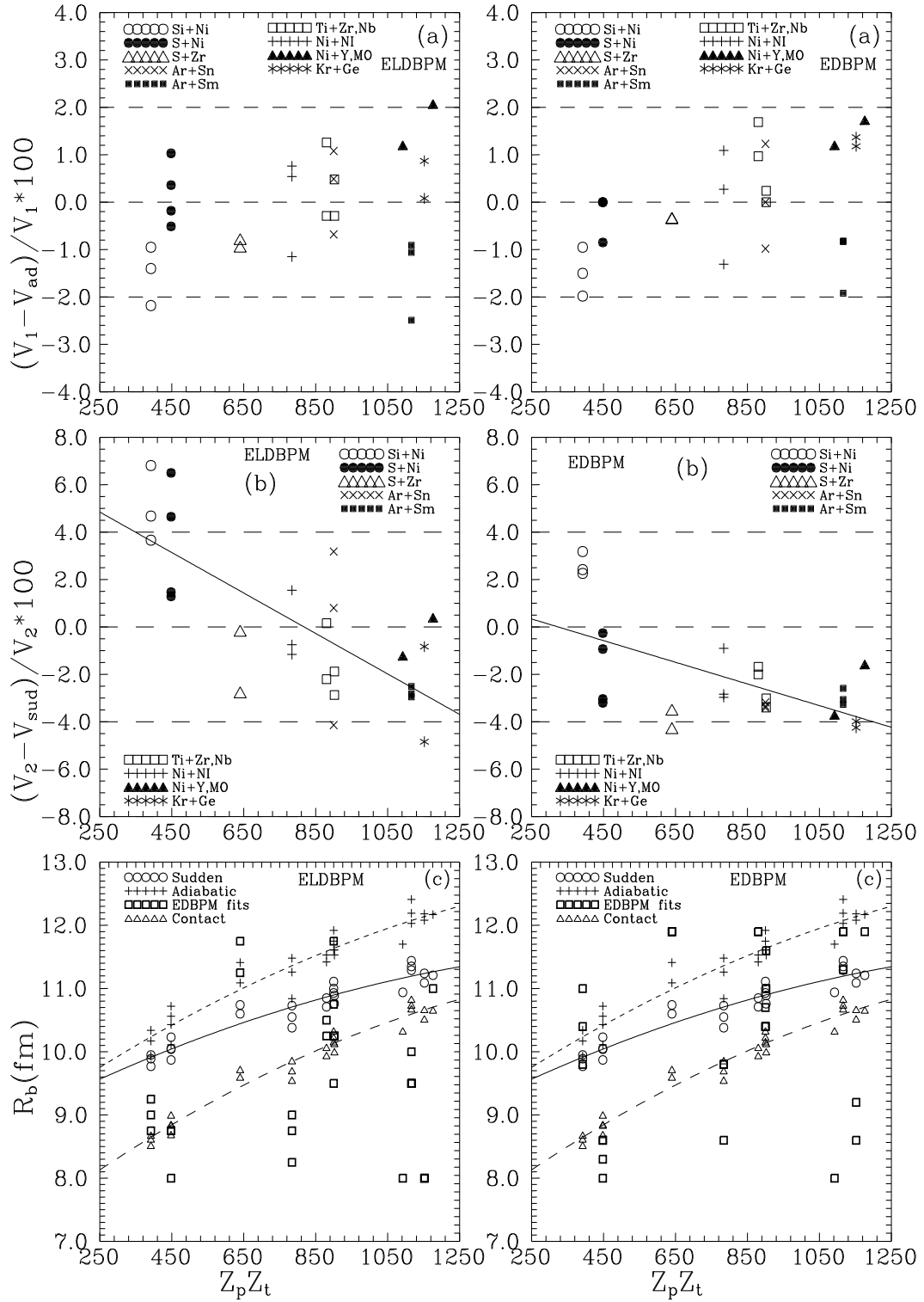


FIG. 3: Percentage deviation of the (a) adiabatic and (b) sudden barriers obtained from empirical prescriptions and the experimental barriers obtained using ELDBPM method. The systems shown by various symbols are for various projectiles listed in the table. In part (c), the fusion barrier radius values obtained from ELDBPM, the corresponding sudden values from Vaz et al., the adiabatic values and the contact distance are shown for a comparison. The solid and dashed lines in the figures (a)-(c) are guides to eye as mentioned in the text.